ANL-76-104

CHEMICAL ENGINEERING DIVISION

FAST-NEUTRON DOSIMETRY ANNUAL REPORT

July 1975—June 1976

by

R. R. Heinrich, L. R. Greenwood, R. J. Kennerley,
N. R. Chellew, R. J. Popek, R. L. Malewicki,
F. A. Cafasso, and L. Burris

ARGONNE NATIONAL LABORATORY, ARGONNE, ILLINOIS

Prepared for the U. S. ENERGY RESEARCH
AND DEVELOPMENT ADMINISTRATION
under Contract W-31-109-Eng-38

Printed in the United States of America
Available from
National Technical Information Service
U. S. Department of Commerce
5285 Port Royal Road
Springfield, Virginia 22161
Price: Printed Copy $4.00; Microfiche $3.00

Distribution Category:
Reactor Materials
(UC-20c)

ANL-76-104

ARGONNE NATIONAL LABORATORY
9700 South Cass Avenue
Argonne, Illinois 60439

CHEMICAL ENGINEERING DIVISION

FAST-NEUTRON DOSIMETRY ANNUAL REPORT

July 1975—June 1976

by

R. R. Heinrich, L. R. Greenwood, R. J. Kennerley,
N. R. Chellew, R. J. Popek, R. L. Malewicki,
F. A. Cafasso, and L. Burris

Previous reports in this series

ANL-7977	July—December 1972
ANL-8022	January—June 1973
ANL-8122	July 1973—June 1974
ANL-75-49	July 1974—June 1975

TABLE OF CONTENTS

LIST OF FIGURES

LIST OF TABLES

LIST OF TABLES (contd)

CHEMICAL ENGINEERING DIVISION

FAST-NEUTRON DOSIMETRY ANNUAL REPORT

July 1975—June 1976

by

R. R. Heinrich, L. R. Greenwood, R. J. Kennerley,
N. R. Chellew, R. J. Popek, R. L. Malewicki,
F. A. Cafasso, and L. Burris

ABSTRACT

One of the objectives of the Dosimetry and Damage Analysis Center is to provide standardized dosimetry technology for materials-study programs within the ERDA Division of Magnetic Fusion Energy. Current efforts have included characterization of neutron environments in terms of fluence and spectral distribution for materials experiments conducted at the Lawrence Livermore Laboratory's (LLL) Rotating Target Neutron Source and at the LLL-Davis Cyclograaff. Environment characterization efforts at Brookhaven National Laboratory's High Flux Beam Reactor and those pertaining to an enriched-uranium converter for the ANL CP-5 reactor are also described. The capability of calculating material radiation damage parameters associated with these neutron environments is demonstrated. Average fission yields determined from two fast-neutron irradiations and one thermal-neutron irradiation are compiled for laboratories participating in the Interlaboratory Reaction Rate program. These results are in excellent agreement with literature values. Progress on the development of ^{10}B- and ^{6}Li-loaded liquid scintillation detectors for detecting very low intensity neutrons is presented. Material purification tests and performance tests of scintillation mixtures are described.

SUMMARY

Dosimetry and Damage Analysis Center (DADAC) for DMFE Materials Research

Current activities of DADAC have included (1) characterization of the neutron radiation fields being used in materials study programs of the ERDA Division of Magnetic Fusion Energy (DMFE) and (2) improvement in the methodology required for these characterizations. In addition, the capability of translating dosimetry data to radiation damage parameters has been established. Neutron fluences measured as a function of source distance for three experiments at the Lawrence Livermore Laboratory (LLL) Rotating Target Neutron Source (RTNS) are presented. Detailed radial dosimetry was provided for one of these experiments in which helium production rates and (n,α) cross sections are being studied in several materials. These data will provide the basis for a detailed neutron fluence profile as a function of position from the source axis. Dosimetry for the other RTNS experiments provided source-distance fluences only. Fluence data obtained by means of selected niobium foils were in excellent agreement with LLL measurements.

Results of a cooperative effort with LLL to define the neutron spectral distribution for a new $^{9}Be(d,n)$ target concept for the LLL-Davis cyclograaff are presented. Two foil packets, each consisting of 14 foils, were placed 3.6 mm and 43.6 mm from the source and at zero degrees to the beam axis. The reaction rates determined by means of these foils were used to unfold the neutron spectrum for each position. Results indicate that the neutron flux does not decrease as quickly as $1/R^2$, presumably because of the new, larger beam-spot size. Also, the difference in the two spectral shapes emphasizes the importance of careful dosimetry for irradiations at this facility.

Preliminary results are given for a dosimetry study being conducted in a ^{235}U converter assembly which is irradiated in the ANL CP-5 reactor. Two dosimeter capsules were placed at different positions within the ^{235}U converter, along with a nickel wire, to monitor relative neutron flux gradients. Results obtained from the $^{58}Ni\ (n,p)^{58}Co$ reaction of the nickel wire are presented and indicate a gradient variation of 8% between the two dosimeter locations.

Presented also is a brief discussion of the dosimetry being done at the Brookhaven National Laboratory (BNL) High Flux Beam Reactor (HFBR). This facility is being used for DMFE material testing because of its relatively large neutron energy component above 1 MeV.

The computer code DISCS was used to calculate the displacement rates of niobium and Type 305 stainless steel upon their exposure to the neutron energy spectrum expected from the proposed Argonne Multi-Component Radiation (AMCOR) facility. Hydrogen and helium production rates were also calculated for these materials and this spectrum. Comparison of the data indicates that damage rates in niobium are about an order of magnitude lower than in 305 stainless steel and that the estimated AMCOR damage rate is about a factor of two lower than the achievable rate at the RTNS.

Geometric corrections were calculated for foils irradiated by neutrons produced by 14- and 16-MeV-deuteron bombardment of a beryllium target at the ANL Tandem accelerator. Three foil packets, each containing 13 materials, resulted in 26 reactions per packet. The geometric corrections for these packets indicated that deviations from the $1/R^2$ relationship at close geometries can be as large as 4% and that different reactions have markedly different corrections, even within the same foil. An NBS-type fission chamber was also used in these irradiations, and enabled the anisotropic neutron flux contours and scattering effects around the Be beam stop to be monitored.

Interlaboratory LMFBR Reaction Rate (ILRR) Program

The ANL effort, as well as those of other laboratories in the ILRR program, has been directed toward improving the measurement of absolute fission rates of ^{235}U, ^{238}U, ^{237}Np, and ^{239}Pu. Fission yield data for these isotopes, based on absolute fission counting with the NBS fission chamber for the CFRMF and BIG-10 irradiations, are compiled; the compiled data are from all the participating laboratories. The average fission-yield values for ^{235}U, ^{238}U, and ^{239}Pu have an uncertainty of less than ±2%, except for the fission-product ^{103}Ru for which the data are more discrepant. Fission yields for ^{237}Np for all laboratories was more uncertain, with the uncertainty being in the range of ±3-6% from the mean. The ILRR and ENDF/B thermal neutron fission yields of ^{95}Zr, ^{103}Ru, and ^{140}Ba for ^{235}U are compared. The agreement between the two sets of data is excellent, except in the case of ^{103}Ru, which deviates by almost 8%.

Development of Liquid Scintillation Neutron Detectors

Progress is reported on the development of ^{10}B-loaded liquid scintillators for the detection of very low intensity neutrons. Results are presented on the purification of materials used in preparing the scintillation cells. Results of cell-performance tests are presented for various mixtures in terms of relative light output and pulse-shape discrimination. Results from light intensity tests of a large volume cell (5.1 cm by 15.2 cm) indicate that the mean free path for light through a mixture of trimethyl borate (51.5%), 1-methylnaphthalene (47.5%), and 9,10-diphenylanthracene (1%) is about 12.7 cm. Low-temperature tests were made on several different mixtures; the results indicated that some of the mixtures tested were stable at temperatures as low as $-17 \pm 3°C$.

Work on the development of ^{6}Li-loaded scintillator systems is also reported, and the results of solubility and stability tests on ^{6}Li-salicylate-containing mixtures are presented.

I. DOSIMETRY AND DAMAGE ANALYSIS CENTER FOR DMFE MATERIALS RESEARCH PROGRAMS

(R. R. Heinrich, L. R. Greenwood, R. J. Kennerley, R. L. Malewicki, and R. J. Popek)

The objectives of the Dosimetry and Damage Analysis Center (DADAC) continue to be the establishment of the capability and the coordination of efforts for the standardized measurement and reporting of dosimetry data and damage correlation parameters. These efforts are being made in support of programs of the Materials and Radiation Effects Branch of the Division of Magnetic Fusion Energy (DMFE). Our near-term goal is to characterize experiments on radiation effects in terms of neutron flux, fluence, and spectral distributions. The applicability of existing spectral-unfolding techniques to neutron environments of higher energy has been demonstrated,[1] and emphasis is now being placed on the extension of these techniques to neutron fields that are being used for studies of radiation effects on MFE-related materials. The neutron fields of active interest include the Rotating Target Neutron Source (RTNS) at Lawrence Livermore Laboratory (LLL), the University of California cyclograaff at Davis, the Be(d,n) accelerator at Oak Ridge National Laboratory (ORNL), the Los Alamos Meson Physics Facility (LAMPF) at Los Alamos Scientific Laboratory (LASL), and the EBR-II facility at Argonne National Laboratory (ANL). Current activities include (1) studies to characterize these fields, (2) studies to improve the experimental methodology used in these characterizations, and (3) monitoring (characterizing) specific radiation-effects experiments that are being conducted or planned within these facilities. Particular emphasis is being placed upon monitoring irradiation experiments in a well-documented manner so that, when standardized methods are ultimately established, the dosimetry for these experiments can be reanalyzed and defined in a consistent and reproducible framework.

Another objective of the DADAC is to provide the capability of translating dosimetry data into parameters that correlate more directly with the observed radiation effects on materials. Again, emphasis is being placed upon standardization and documentation, because the methodology to compute damage-correlation parameters and the optimal parameters themselves are not yet well established. Damage-correlation parameters that are currently being used to interpret radiation effects include primary knock-on atoms (PKA), displacements per atom (dpa), helium production, and nuclear transformations.

It has been postulated that energetic plasma radiations striking the first wall of a fusion reactor could lead to serious wall erosion and, possibly, to plasma contamination. For this reason, the erosion of surfaces of various materials (*e.g.*, Nb, V, stainless steel, Al, and Si) have been studied under bombardment of 14-MeV neutrons by several experimenters.[2-5] The principal efforts of DADAC this year have focused on providing neutron dosimetry for experiments of this type, and on the development of dosimetry techniques applicable to Be(d,n) irradiation facilities.

A. Neutron Dosimetry for the Rotating Target Neutron Source (RTNS) at Lawrence Livermore Laboratory

(R. R. Heinrich and R. L. Malewicki)

The Rotating Target Neutron Source (RTNS) at Lawrence Livermore Laboratory is being used to irradiate MFE-related materials in studies of surface-particle

release, as well as in studies of bulk damage. The RTNS produces neutrons by fusion of deuterium and tritium:

$$D + T \rightarrow n + He + 18\ MeV$$

The neutrons produced are nominally 14 MeV, but the exact energy depends on the deuteron energy and the angle between the path of the incoming deuteron and the path of the emitted neutron. For the RTNS, the calculated neutron energy can range from 13.2 MeV at an angle of 180° to 15.1 MeV at an angle of 0°.[6] The localized source of neutrons at the target consists of a disc-shaped region that is a few millimeters in diameter and of negligible thickness. The uniformity of the neutron yield across the target spot is affected by variations in the current density of the deuteron beam and by variations in the tritium loading of the target. However, because the target is rotated and scanned rapidly, this latter effect is negligible, and the neutron yield is directly proportional to the beam current density. Because of the small size of the neutron spot source, the neutron flux decreases rapidly, both radially and axially, as the distance from the source increases; and, for this reason, dosimetry is necessary in any experiment on the RTNS machine.

A group of samples consisting of twelve pure elements was irradiated in the RTNS in May 1975 as part of an Atomics International (AI) research investigation to determine the helium generation rates and spectrum-averaged (n,α) cross sections of materials that may find application in the Magnetic Fusion Energy program. The need to know the neutron-fluence variation precisely over the volume occupied by these samples led to the design of detailed dosimetry procedures for this experiment.

The irradiation assembly used in this experiment is shown in Fig. I-1. Multiple helium-generation specimens of ten pure elements (C, Al, Ti, V, Fe, Ni, Cu, Zr, and Mo) and Type 316 stainless steel were sandwiched between two stacks of dosimeter foils. These materials were packaged in a 2.54-cm-square, 1.6-mm-thick stainless steel plate with concentric holes milled out of the center to hold the various components and provide alignment of the foils. Single sheets of 0.13-mm-thick Type 316 stainless steel were spotwelded to the front and back to hold the package together, resulting in a total package thickness of about 1.9 mm.

The radiometric dosimetry foils consisted of three sets of Au, Nb, and Ni foils prepared from material supplied by our Laboratory. Two sets of thin foils (designated "front" and "middle" respectively) sandwiched the helium-generation specimens and a third set of thicker foils (designated "back") was located behind the sandwich. The back set, which also included Fe and Pt foils, was intended principally for helium generation measurements, but the Au, Nb, and Ni foils were first analyzed radiometrically. The gold foils provided dosimetry information by means of the $^{197}Au(n,2n)^{196}$ Au reaction, which was the primary basis of the fluence profile information because the high activities allowed segmenting into smaller pieces for counting. The segmenting procedure provided the information needed to map the neutron fluence profile as a function of distance from the neutron source axis, and the niobium foils provided a redundancy check on this information. The nickel foil activities were used to determine the average energy of the neutron beam by comparing the energy-sensitive ratio of the $^{58}Ni(n,p)^{58}Co$ and $^{58}Ni(n,2n)^{57}Ni$ cross sections.

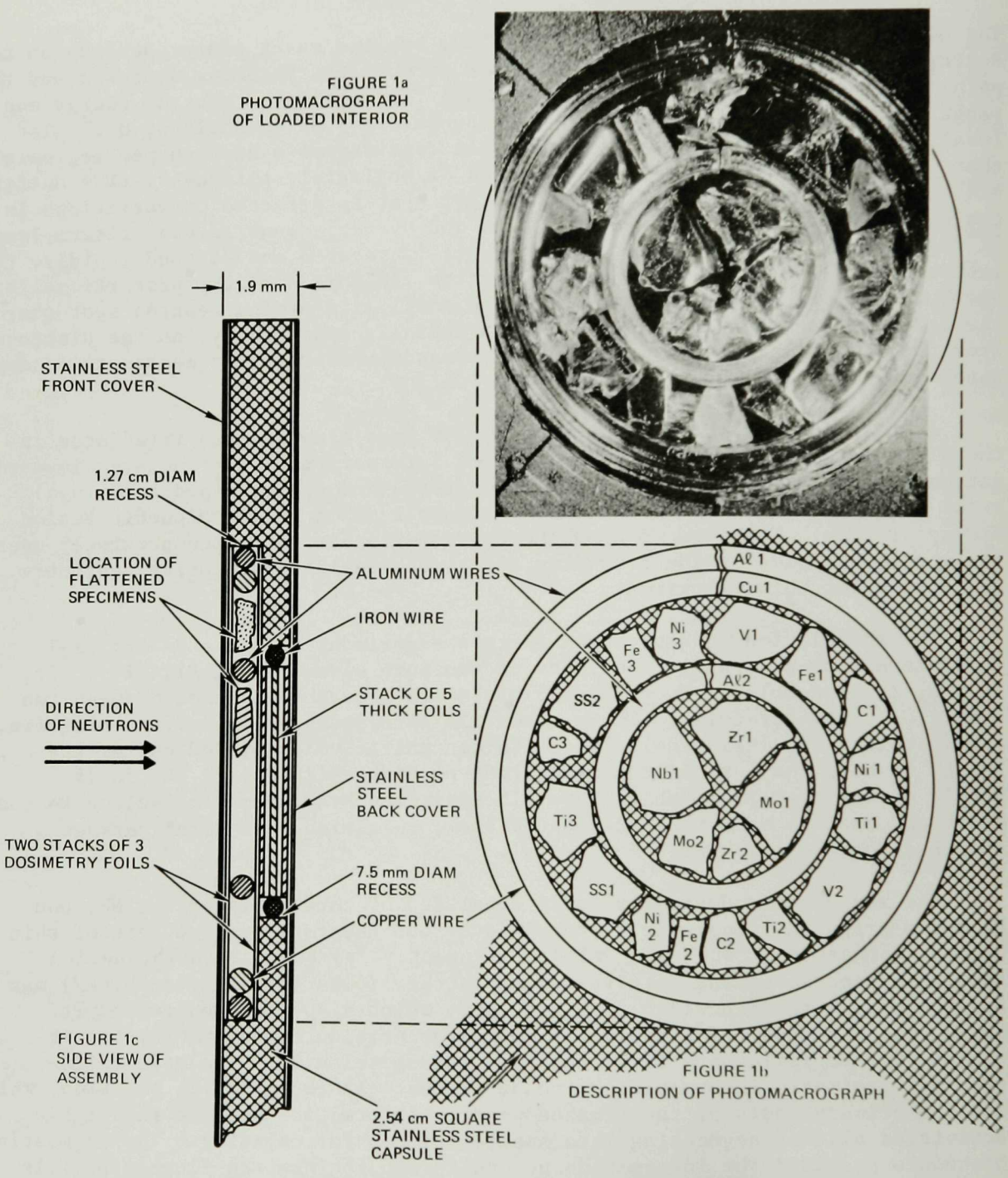

Fig. I-1. RTNS Irradiation Assembly. (Courtesy of Atomics International)

The assembled package was mounted directly on the RTNS chamber wall, and irradiated for 77.55 hr within the period of May 19-24, 1975. (This experiment was run in tandem with an ANL irradiation experiment of M. Kaminsky,* whose apparatus immediately followed the AI package.) After a short post-irradiation waiting period to allow for the decay of high-level, short-lived activities in the vicinity of the beam-stop, the package was disassembled. The nine dosimetry foils were then segmented along lines that had been scribed earlier. The geometries of the segmented foils are shown in Figs. I-2 and I-3. In these diagrams, the 0° neutron beam is directed into the paper. The Ni and Au foil segments were immediately shipped to ANL for radiometric counting and weighing. The Nb segments were counted at LLL and then shipped to ANL for further counting and weighing. All foils were subsequently shipped to AI, where they were reweighed and stored for later helium analysis.

The average neutron fluences intercepted by the individual foil segments were calculated from the measured foil weights, foil activities, and irradiation history. The irradiation history was obtained from the output of two proton recoil counters used as monitors during the experiment. Two of the nuclear parameters used in the calculations, the residual nuclei half-lives and the reaction cross-sections, are listed in Table I-1. The average fluences calculated for the 62 dosimetry foil segments, along with their relative uncertainties, are listed in Tables I-2 and I-3.

The tabulated values omit the uncertainties in the evaluated cross-sections, and hence must not be used in an absolute sense to the accuracy shown. However, relative accuracies, and, therefore, relative energy variations from segment to segment, are much less dependent on these cross-section uncertainties. Examination of the ^{93}Nb(n,2n) and ^{197}Au(n,2n) cross-section measurements in the 14 MeV region[8,9] showed relatively flat energy dependencies, and the data scatter was such that constant cross-section values were adopted.[10]

Close examination of the fluence results shows a consistent nonisotropic distribution about the centers of the foils. This indicates that the incident neutron beam was not exactly centered on the helium-generation package. Comparison of the fluences for successive foils in each of the three dosimetry sets shows some inconsistency, indicating, perhaps, that an inconsistency may exist in the cross-sections adopted in Table I-1 for the dosimetry reactions. Also, for comparison, the neutron fluences determined from the dosimeter foils from the Kaminsky apparatus are presented in Table I-4, together with the data from the centermost foil pieces from the AI irradiation package. Data for the AI front gold foil consist of average fluences for the five centermost segments; for the back gold foil, the data represent average fluences for the four centermost segments. Data for the far back nickel and niobium foils also represent fluence averages for four segments. From the data presented, cross-section discrepancies appear to exist primarily for the ^{58}Ni(n,p)^{58}Co reaction: that is, fluence values obtained from this reaction appear to be high relative to the gold and niobium reactions and indicate that the value of the ^{58}Ni(n,p) cross section may be about four percent low at this neutron energy.

*Member of Argonne's Physics Division.

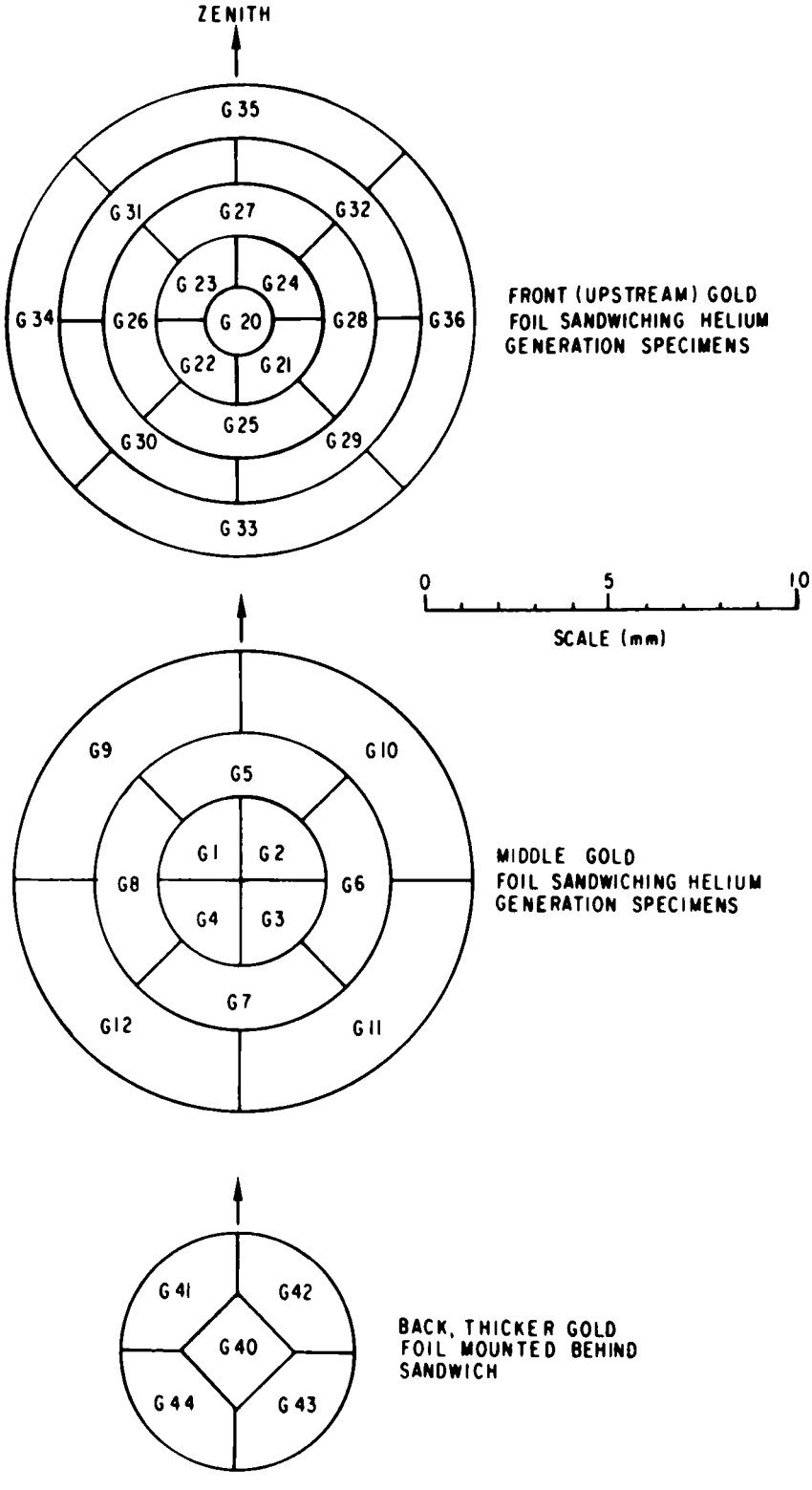

Fig. I-2. Orientation and Geometry of RTNS-Irradiated Gold Dosimetry Foil Segments

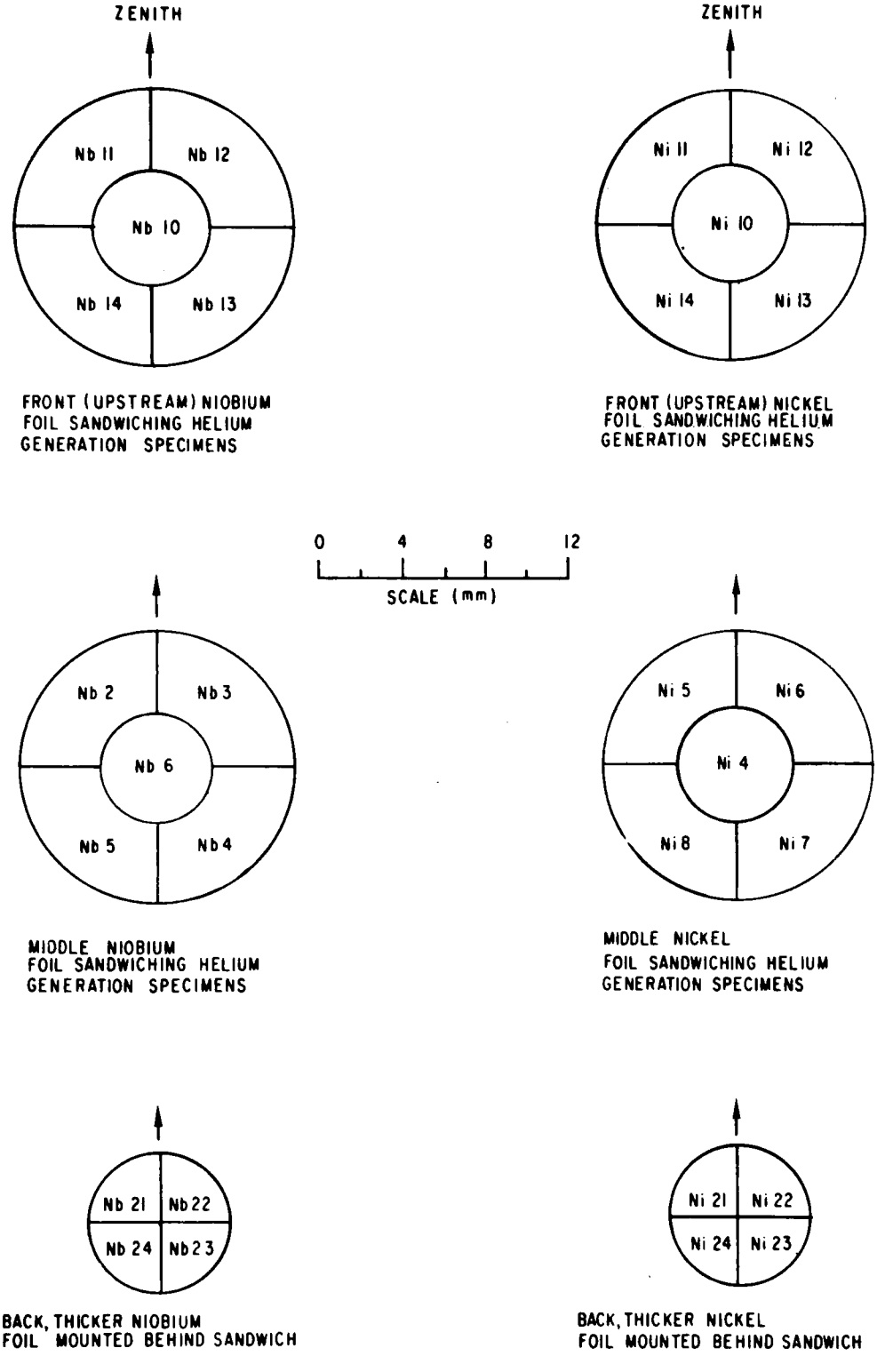

Fig. I-3. Orientation and Geometry of RTNS-Irradiated Niobium and Nickel Dosimetry Foil Segments

Table I-1. Nuclear Parameters Used in the Neutron Fluence Calculations

Reaction	Half-Life	Spectrum-Averaged Cross-Section
$^{197}Au(n,2n)^{196}Au$	6.183 d	2110 mb
$^{93}Nb(n,2n)^{92m}Nb$	10.16 d	458 mb
$^{58}Ni(n,p)^{58}Co$	71.23 d	329.4 to 316.0 mb[a]
$^{58}Ni(n,2n)^{57}Ni$	1.50 d	35.0 to 37.5 mb[a]

[a]Energy-dependent values were interpolated from the ENDF/B-IV dosimetry file (Ref. 7).

Table I-2. Average Fluences Calculated for RTNS-Irradiated Gold Foil Segments

Foil Location	Segment Number	Average Fluence, 10^{17} n/cm^2	Foil Location	Segment Number	Average Fluence, 10^{17} n/cm^2
Front	G20	2.568 ± 0.024	Middle	G1	1.968 ± 0.019
	G21	2.517 ± 0.027		G2	1.969 ± 0.020
	G22	2.505 ± 0.026		G3	2.039 ± 0.014
	G23	2.406 ± 0.025		G4	2.053 ± 0.020
	G24	2.454 ± 0.024		G5	1.683 ± 0.014
	G25	2.413 ± 0.032		G6	1.831 ± 0.017
	G26	2.242 ± 0.020		G7	1.818 ± 0.016
	G27	2.068 ± 0.018		G8	1.789 ± 0.016
	G28	2.328 ± 0.020		G9	1.362 ± 0.014
	G29	2.151 ± 0.028		G10	1.360 ± 0.012
	G30	2.033 ± 0.019		G11	1.577 ± 0.013
	G31	1.846 ± 0.025		G12	1.476 ± 0.019
	G32	1.866 ± 0.019			
	G33	1.742 ± 0.015	Back	G40	1.731 ± 0.011
	G34	1.629 ± 0.015		G41	1.572 ± 0.010
	G35	1.420 ± 0.015		G42	1.624 ± 0.011
	G36	1.739 ± 0.015		G43	1.764 ± 0.011
				G44	1.730 ± 0.010

Table I-3. Average Fluences Calculated for RTNS-Irradiated Niobium and Nickel Foil Segments

Niobium			Nickel			
Foil Location	Segment Number	Average Fluence, 10^{17} n/cm^2	Foil Location	Segment Number	Average Fluence, 10^{17} n/cm^2	Neutron Energy, MeV[a]
Front	Nb-10	2.472 ± 0.018	Front	Ni-10	2.266 ± 0.013	14.92 ± 0.02
	Nb-11	1.764 ± 0.013		Ni-11	1.662 ± 0.014	14.88 ± 0.03
	Nb-12	1.834 ± 0.013		Ni-12	1.627 ± 0.014	14.85 ± 0.03
	Nb-13	2.136 ± 0.015		Ni-13	1.952 ± 0.011	14.86 ± 0.02
	Nb-14	1.988 ± 0.014		Ni-14	1.840 ± 0.014	14.79 ± 0.03
Middle	Nb-2	1.429 ± 0.010	Middle	Ni-4	1.820 ± 0.015	14.96 ± 0.03
	Nb-3	1.404 ± 0.010		Ni-5	1.318 ± 0.012	14.91 ± 0.03
	Nb-4	1.654 ± 0.012		Ni-6	1.389 ± 0.012	14.89 ± 0.03
	Nb-5	1.555 ± 0.011		Ni-7	1.567 ± 0.013	14.91 ± 0.03
	Nb-6	1.950 ± 0.014		Ni-8	1.442 ± 0.013	14.89 ± 0.03
Back	Nb-21	1.519 ± 0.010	Back	Ni-21	1.624 ± 0.012	14.98 ± 0.03
	Nb-22	1.485 ± 0.010		Ni-22	1.652 ± 0.010	14.96 ± 0.02
	Nb-23	1.617 ± 0.011		Ni-23	1.768 ± 0.008	14.96 ± 0.02
	Nb-24	1.593 ± 0.011		Ni-24	1.716 ± 0.008	15.00 ± 0.02

[a]Neglecting ENDF/B-IV cross-section uncertainties for the ^{58}Ni(n,2n) and ^{58}Ni(n,p) reactions.

Table I-4. Neutron Flux and Fluence Determined From AI and Kaminsky Dosimeter Foils

Dosimeter Foil	Experimenter Identity	Distance from Source, mm	Average Fluence, 10^{17} n/cm^2
Nb (Front)	AI	4.0	2.49
Ni		4.03	2.61
Au		4.04	2.53
Au (Middle)	AI	4.81	1.98
Ni		4.84	2.08
Nb		4.85	1.92
Ni (Back)	AI	6.69	1.92
Au		6.72	1.65
Nb		6.73	1.56
Ni	Kaminsky	6.80	0.981
Au		6.83	0.789
Nb		6.84	0.727

Since this study represents the most detailed fluence profile yet obtained for the RTNS, we intend to use these data to develop a mathematical model for the purpose of obtaining a neutron fluence at any zero-degree beam position at the RTNS.

The RTNS facility has also been used for studies of bulk radiation damage in materials. Members of Argonne's Materials Science Division (C. Merkle and R. Lyles) are studying the cascade process in silver and copper crystals that is initiated by primary knock-on atoms when bombarded by 14-MeV neutrons. Dosimetry was provided for a bulk-damage experiment of Merkle and Lyles, whose samples were irradiated at the RTNS on June 20, 1975. The irradiation package comprised two copper capsules which were approximately 9.5-mm in diameter but of different lengths, one being 70 mm long and the other, 105 mm long. The shorter capsule was scribed 28 mm from the front end, the mark indicating the approximate position of the specimens farthest from the neutron beam. This position was similarly marked on the long capsule at 56 mm from the front face. Both capsules were taped to a 9.5-mm dia iron rod with the front faces exactly flush, and this assembly was positioned so that the front faces were 12 mm from the RTNS target. The total beam time was relatively short (4.25 hr).

Dosimetry foils of Nb, Ni, and Au were located inside each capsule and were strategically placed before and after the silver and copper microscopy specimens. Additional niobium dosimetry foils were placed outside each capsule by LLL; the outside Nb foils were located on the front face and at the scribed position of each capsule. All the foils at the scribed positions were perpendicular to the direction of the neutron beam. Flux and fluences determined from the interior dosimetry foils are summarized in Table I-5, along with the fluences from the exterior LLL Nb foils. Foil identifications are in accordance with the Materials Science Division designations; the Vac designation corresponds to the short capsule, and the He designation to the longer capsule.

Table I-5. Flux and Fluences From the RTNS Irradiation of June 20, 1975

Foil Identification	Distance from RTNS Target, mm	Average Fluence, 10^{14} n/cm^2
Nb-F-Vac	12.1	28.1
Nb-410(LLL)	12.0	28.6
Nb-1-Vac		14.5
Au-1-Vac	17.1	13.9
Ni-1-Vac		13.0
Nb-2-Vac		2.25
Au-2-Vac	37.7	2.25
Ni-2-Vac		2.24
Nb-432(LLL)	36	2.32
Nb-F-He	12.1	26.0
Nb-431(LLL)	12.0	26.3
Au-1-He	17.1	10.8
Ni-1-He		10.5
Nb-2-He		2.68
Au-1-He	36.7	2.69
Ni-2-He		2.55
Nb-3-He		1.57
Au-3-He	41.5	1.57
Ni-2-He		1.57
Nb-433(LLL)	68	0.70

Comparison of the results in Table I-5 indicates exceptionally good agreement between the various foil fluences, including those obtained by Lawrence Livermore Laboratory (LLL).

During the period from January 12, 1976 to January 17, 1976, the sixteenth experiment in a series of Kaminsky surface-study irradiation experiments was conducted at the RTNS. The total irradiation time was 108.1 hr, with an actual beam time of 78.3 hr. Dosimeter foils of Ni, Au, and Nb were supplied and affixed to the face of the Kaminsky apparatus at approximately 4 mm from the source of neutrons. Center alignment of the foils was at zero degrees to the neutron beam with a stacking order of Ni, Au, and Nb relative to the forward direction of the neutrons. The estimated total fluence was approximately that obtained in the previous Kaminsky-Atomics International experiment, namely $\sim 1 \times 10^{17}$ n/cm^2.

The foils were received approximately one week after the irradiation; however, because of the high fluence level, the 36-hr ^{57}Ni activity was still intense enough to allow counting, and enabled us to determine the average neutron energy by the $^{58}Ni(n,p)/^{58}Ni(n,2n)$ spectral index. Summarized in Table I-6 are the fluxes, fluences, and neutron energy determined from the dosimetry foils used in this irradiation. The neutron energy determined from the Ni spectral index was 14.8 MeV, which confirms the energy predicted from the kinematics of the DT fusion reaction. Because the flux intensity decreases as the distance from the neutron source increases, the higher induced activity in the gold foil suggests that an experimental error occurred in the data or that an error was made in the stacking order of the foils. The ratio of the gold (n,2n) to (n,γ) reaction rates is about 200, which indicates that very little neutron scattering occurred during this irradiation.

Table I-6. KAM-16 Irradiation at RTNS on January 12-17, 1976. E_n = 14.8 MeV

Target Nucleus	Reaction	Reaction Rate	Average Fluence, 10^{17} n/cm^2
^{58}Ni	n,2n	1.11×10^{-14}	1.20
^{58}Ni	n,p	9.37×10^{-14}	1.18
^{197}Au	n,γ	3.26×10^{-15}	
^{197}Au	n,2n	6.98×10^{-13}	1.29
^{93}Nb	n,2n	1.31×10^{-13}	1.11

B. Neutron Dosimetry at the University of California-Davis Cyclograaff (L. R. Greenwood and R. R. Heinrich)

Surface-erosion and bulk-damage material studies are also being conducted at the University of California cyclograaff in Davis, California. This facility consists of a cyclotron and a Van de Graaff generator used in tandem. Bunched negative deuterium ions are produced in and accelerated by the cyclotron to a slit at the entrance of the Van de Graaff generator. These beam pulses are additionally accelerated by the Van de Graaff to the desired deuteron energy and then focused on a thick beryllium target to produce neutrons by the reaction $^{9}Be(d,n)^{10}B$. The thick beryllium target is mounted on a tantalum plate, and this assembly is contained in a cylindrical brass chamber that is electrically insulated so that beam currents can be measured and integrated. The average neutron energy produced by this reaction is approximately 0.4 times the incident deuteron energy at zero degrees to the beam.

On October 16, 1975, an experiment was conducted at the cyclotron of the University of California at Davis in cooperation with R. Van Konynenburg and other members of Lawrence Livermore Laboratory (LLL). A variety of foils were irradiated at two distances (3.6 mm and 43.6 mm) behind the beam stop, which was designed by LLL. The design of this device was such that the deuteron beam

was swept across the target in order to reduce the pronounced variations in neutron flux and spectra that are characteristic of this type of source. The irradiation, at a deuteron energy of 30 MeV, had an average current of 20 μA for 72 min, and resulted in a total charge of 0.0865 coulomb.

The foils used and the reactions measured in this experiment are listed in Table I-7. Activities were measured at LLL and corrections were made for variations in geometry ($1/R^2$). The measured activity data were sent to ANL and were used as input to the SAND-II spectrum-unfolding code. The cross-section library of SAND-II was modified to extend its energy range to 30 MeV and to include the new reactions used in this experiment.

Table I-7. Foils and Reactions Used for the University of California-Davis Irradiations

$^{27}Al(n,\alpha)^{24}Na$	$^{89}Y(n,3n)^{87}Y$
$^{45}Sc(n,2n)^{44m}Sc$	$^{90}Zr(n,2n)^{89}Zr$
$^{54}Fe(n,\alpha)^{51}Cr$	$^{169}Tm(n,2n)^{168}Tm$
$^{54}Fe(n,p)^{54}Mn$	$^{169}Tm(n,3n)^{167}Tm$
$^{56}Fe(n,p)^{56}Mn$	$^{197}Au(n,2n)^{196}Au$
$^{59}Co(n,2n)^{58}Co$	$^{197}Au(n,3n)^{195}Au$
$^{89}Y(n,2n)^{88}Y$	$^{197}Au(n,4n)^{194}Au$

The unfolded spectra are shown in Fig. I-4. As can be seen, there are pronounced variations in both flux and spectra between the two locations behind the beam stop. The flux does not appear to decrease as quickly as is indicated by $1/R^2$, presumably because of the large size of the effective beam spot (5 cm high by 11 mm long) and the size of the foils (1.6 mm by 6.4 mm long for the front foils and 13 mm by 6.4 mm long for the rear foils). The spectral changes are caused by the difference in angles intercepted by the foils (±40° for the front packet and ±4° for the rear packet) and illustrates the importance of adequate dosimetry for evaluating neutron spectra at close geometries.

In the future, we plan to make similar measurements at the Davis and the Oak Ridge accelerators and, if possible, we shall include time-of-flight or other differential measurements in order to evaluate the validity of the neutron cross sections used in the spectral-unfolding method.

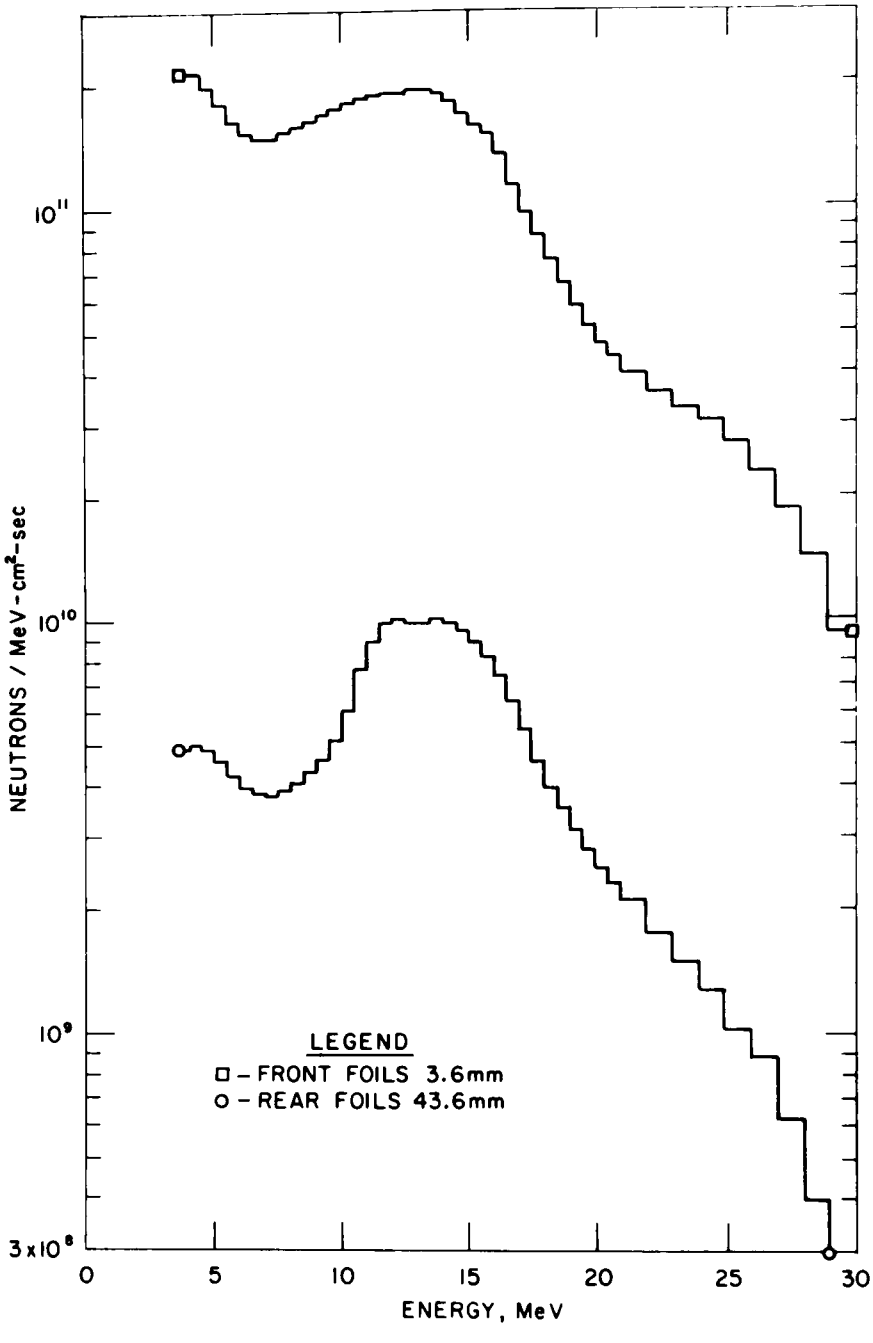

Fig. I-4. SAND-II Neutron Spectra for University of California-Davis Irradiation: 30 MeV Deuterons on Beryllium

C. Characterization of the VT-53 Converter Neutron Environment

(R. R. Heinrich and R. L. Malewicki)

As a cooperative effort between the DADAC and the Material Science Division (MSD), the neutron environment inside the VT-53 ^{235}U converter is being determined in terms of flux and spectrum by the foil activation technique. The converter is being used as a source of neutrons for the study of material damage and sputtering effects in a fission neutron environment. These studies are carried out at the ANL CP-5 reactor, utilizing the thermal neutrons to induce fission within the converter. The converter fits into a vertical hole in the reactor and is cooled by a liquid helium cryostat during an irradiation.

Counting is in progress of dosimeter foils contained in two capsules located 7.14 and 19.2 cm from the bottom of the cryostat; these locations cover the area used for MSD experiments. In addition to these dosimeter foils, a nickel wire, which extended 45.7 cm upward from the bottom of the cryostat, was counted to determine flux gradients. Presented in Table I-8 are relative reaction rates of one-inch segments of the nickel wire as a function of axial distance from the bottom of the VT-53 cryostat. From these data, only about an 8% variation in flux is expected at the locations of the dosimeter capsules.

Table I-8. Nickel Activity Gradients in the VT-53 Converter

Sample	Distance from Bottom of Cryostat, cm	Relative Activity, 10^5 dpm/mg
KBC-G-1	2.54	11.2
-2	5.08	11.4
Dosimeter Capsule	7.14	-
KBC-G-3	7.62	11.1
-4	10.2	11.2
-5	12.7	11.2
-6	15.2	11.0
-7	17.8	10.7
Dosimeter Capsule	19.2	-
KBC-G-8	20.3	10.1
-9	22.9	9.55
-10	25.4	8.72
-11	27.9	7.56
-12	30.5	6.04
-13	33.0	4.21
-14	35.6	2.84
-15	38.1	1.91
-16	40.6	1.32
-17	43.2	0.938
-18	45.7	0.703

D. Characterization of the Irradiation Environment of the High Flux Beam Reactor (HFBR)
(R. R. Heinrich and R. J. Popek)

In response to a request by Brookhaven National Laboratory (BNL) for dosimetry assistance at the High Flux Beam Reactor (HFBR), a cooperative experimental effort has been initiated to characterize this environment. The estimated flux is approximately 3×10^{14} n/cm^2-sec, with about 40% being in the thermal energy range. Scoping calculations have indicated that an 8- to 16-hr irradiation would be adequate for this determination. Monitoring will be done over an axial distance of about 45.7 cm; multiple dosimetry foils contained in four aluminum capsules will be used.

Welding and shipping of the capsules to BNL were carried out in April 1976. Prior to shipping, the welded capsules were leak-tested at 200°C for 15 min to ensure the integrity of the weld during irradiation. The irradiation was conducted on April 28, 1976, for a 16-hr period, after which the capsules were removed and allowed to cool before shipping to ANL, where counting and analysis are in progress.

E. Damage Analysis
(L. R. Greenwood, R. J. Kennerley, G. R. Odette,* and R. R. Heinrich)

An important source of irradiation damage in materials is the displacement of atoms from their normal lattice sites as the result of neutron-nuclear interactions. Fast-neutron interactions produce primary knock-on-atoms (PKA) which result in a chain of secondary recoiling atoms that approach a minimum energy needed to cause an atomic displacement. Displacements per atom (dpa) are the irradiation exposure units widely used to correlate neutron damage data and can be expressed by

$$\text{dpa} = t \int_0^\infty \phi(E)\sigma_d(E)\, dE \qquad (1)$$

where: $\phi(E)$ is the differential neutron flux, n/cm^2-sec,
$\sigma_d(E)$ is the displacement cross section, cm^2, and
t = time

The displacement cross section is used to relate the number of displaced atoms from all significant reactions to a particular neutron energy, and is given by

$$\sigma_d(E) = \sum_x \sigma_X(E) \int_{T-}^{T+} K(E,T)_X \nu(T)\, dT \qquad (2)$$

where: E = incident neutron's energy in the laboratory system,
T = recoil nucleus energy in laboratory system,
$\sigma(E)$ = reaction cross section at energy E,
$K(E,T)_X$ = energy transfer kernel,
$\nu(T)$ = secondary displacement function or model, and
X = reaction type

*Consultant, Dept. of Chem. and Nucl. Engineering, University of California, Santa Barbara.

K(E,T) represents the probability that an incident neutron of energy E will produce a primary knock-on atom, or PKA, of energy T, in the laboratory system. The term $\nu(T)$ is a theoretical secondary displacement model which describes the number of atoms that will be ejected from their lattice sites owing to the PKA.

The computer code DISCS[11] (*DIS*placement *C*ross *S*ection) calculates energy-dependent displacement cross sections and PKA distributions for various neutron reactions and secondary displacement models. Neutron reactions handled by the DISCS code are elastic, inelastic, (n,2n), and (n, charged particle). Secondary displacement models available are those of Lindhard *et al.*,[12] Kinchen and Pease,[13] and/or a user-supplied model.

The DISCS code has been used to calculate damage parameters for the proposed Argonne Multi-Component Radiation (AMCOR) facility. This facility would be located at the ANL Cyclotron and would utilize the 22-MeV deuteron beam to produce neutrons by the ^{9}Be(d,n) reaction. We have estimated the neutron spectrum (Fig. I-5) for this facility from our previously measured ^{9}Be(d,n) tandem accelerator spectra. The displacement rate (dpa/sec) for niobium has been calculated using DISCS for this neutron distribution, and these data are compared with those for other facilities in Table I-9. Based on the niobium spectrum-averaged cross sections in Table I-10, production rates of hydrogen and helium gas were also calculated for niobium. Similar calculations were made for Type 305 stainless steel, and these results are presented in Table I-11, along with the spectrum-averaged cross sections used in the calculations.

The data in Table I-9 indicate that irradiation times would have to be increased by a factor of about two at the AMCOR to achieve niobium damage rates comparable to those at the RTNS (14-MeV). A comparison of the estimated damage in niobium and Type 305 stainless steel (Table I-11) indicates that niobium exhibits less damage defects than does Type 305 stainless steel by about one order of magnitude.

On the basis of earlier sensitivity studies,[17] an effort was initiated to experimentally evaluate potential dosimetry-type cross sections in the energy range of 6-12 MeV. The approach has been to measure, by the time-of-flight (T-O-F) technique, the differential neutron flux used for the irradiation of various dosimetry materials. The differential neutron flux, $\phi(E)$, is produced by bombarding a thick beryllium target with deuterons of a known energy. Dosimetry foils are exposed to the neutron flux, and the activity of the foil material transmutants, $\langle\sigma\phi\rangle_{exp}$, is measured by absolute Ge(Li) counting. The evaluation of the differential cross section, $\sigma(E)$, is established by the equality

$$\langle\sigma\phi\rangle_{exp} = \int_0^{E_{max}} \sigma(E)\phi(E)\, dE \qquad (3)$$

This first experiment[17] utilized the Argonne tandem accelerator and consisted of two deuteron irradiations of 14 and 16 MeV on thick Be targets.

A second series of neutron irradiation experiments was conducted at the Argonne tandem accelerator from March 30-April 1, 1976. A collimated deuteron beam of about 1 μA at energies of 14 and 16 MeV was stopped by a 0.6 cm-thick disc of beryllium. This produced a continuous neutron spectrum--from the

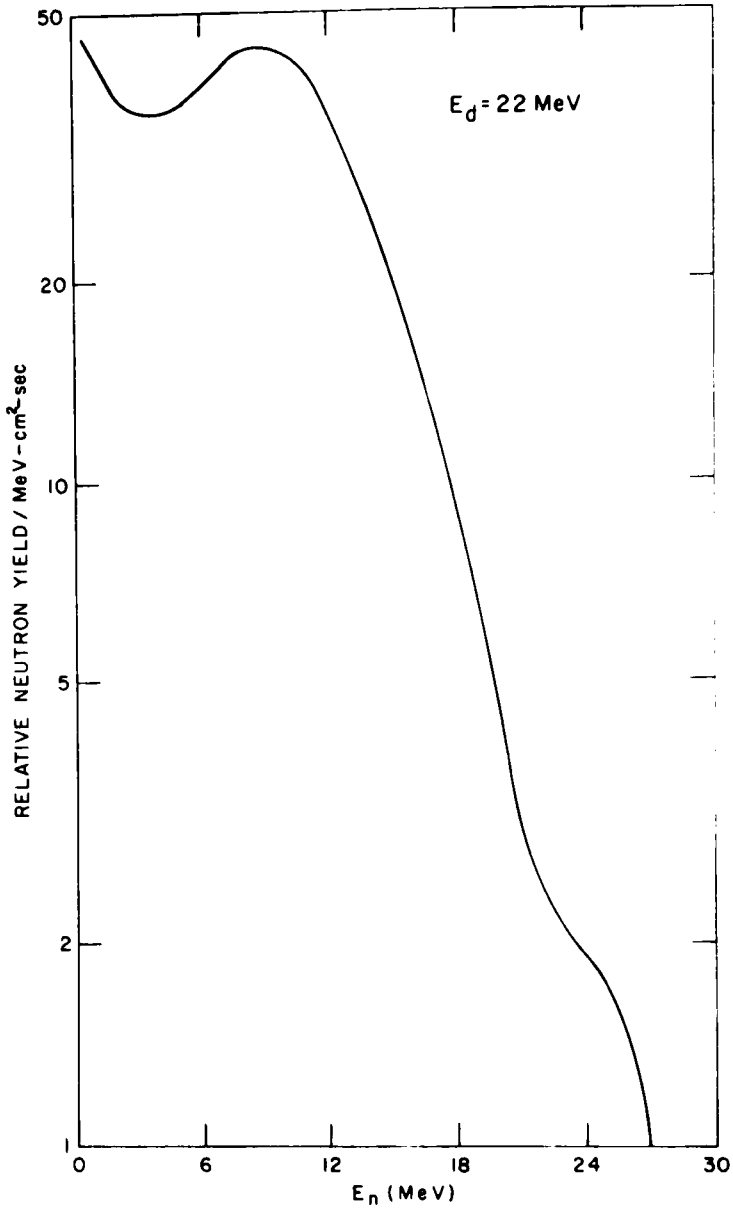

Fig. I-5. Estimated Neutron Spectrum for AMCOR

Table I-9. Comparison of Niobium Damage Parameters in Various CTR Environments

Facility	dpa/sec	Helium, ppm/sec	Hydrogen, ppm/sec	Flux, n/cm^2-sec
AMCOR [Be(d,n)] E_d = 22 MeV	3.36×10^{-9}	6.44×10^{-9}	3.93×10^{-8}	2×10^{12}
CTR First Wall (Ref. 14)	2.11×10^{-7}	4.00×10^{-7}	---	2×10^{14}
14 MeV[a] (Ref. 14)	6×10^{-9}	2×10^{-8}	---	2×10^{12}
Li(d,n) (Ref. 14) E_d = 30 MeV	2.7×10^{-7}	6.5×10^{-7}	---	1×10^{14}

[a] Equivalent to RTNS energy.

Table I-10. Niobium Spectrum-Averaged Cross Sections

Facility	$\langle\sigma_{n,\alpha}\rangle$ mb	$\langle\sigma_{n,p}\rangle$ mb
AMCOR [Be(d,n)] E_d = 22 MeV	3.21[a]	17.36
UWMAK-I First Wall (Ref. 15)	2.3	10.4
14 MeV (Ref. 15)	9.2	40
Li(d,n) (Ref. 16) E_d = 18.5	3.24	14.2
Li(d,n) (Ref. 16) E_d = 24.5	4.83	18.9

[a] (n,α) contribution only; (n,n',α) would increase magnitude by ∿30% in this spectrum.

Table I-11. Estimated Damage Parameters for Type 305 Stainless Steel at the AMCOR Facility [Be(d,n), E_d = 22 MeV][a]

dpa/sec	Helium, ppm/sec	Hydrogen, ppm/sec	Flux n/cm^2-sec
4.5×10^{-9}	5.2×10^{-8}	2.2×10^{-7}	2×10^{12}

[a] The spectrum-averaged cross sections used in the calculations were as follows: $\langle\sigma_{dam}\rangle_{b\text{-}eV} = 2.2 \times 10^5$; $\langle\sigma_{n,\alpha}\rangle_{mb} = 25$; and $\langle\sigma_{n,p}\rangle_{mb} = 108$.

$^{9}Be(d,n)$ reaction and deuteron breakup--extending from thermal energies up to about 20 MeV, with a median energy of 5-6 MeV.

Three foil packets, each consisting of thirteen materials, were irradiated and each produced 26 activation products. These integral measurements will be compared to our previous T-O-F spectral measurements in order to test the accuracy and consistency of the neutron activation cross sections.

The NBS-type fission chamber was also used in this irradiation in order to obtain four types of information. The NBS-type fission chamber is a double chamber loaded with both ^{235}U and ^{238}U deposits (on platinum) in a back-to-back arrangement. First, the chamber was used to monitor the integration of the deuteron beam in order to verify the irradiation history. Secondly, the small size of the deposits (1.27-cm dia) allowed us to map the highly anisotropic neutron-flux contours around the beam stop. Thirdly, various thicknesses of materials were placed around the chamber to measure scattering absorption. These studies indicated that neutron scattering was minimal at distances close to the beam stop, except when hydrogenous material was used. In this case the effect of thermal neutrons on the fission counter was significant. These studies also allowed us to measure absorption by the foil packets themselves so that corrections could be made for this effect. Finally, the absolute number of fissions measured by the fission counter will allow us to determine fission yields from the larger foils of ^{235}U and ^{238}U placed in the foil packets.

Most of the irradiated foil materials have been gamma-counted, using our Ge(Li) detectors. The measured activities were converted to saturated activities in order to compare them with activities calculated from our time-of-flight neutron spectrum and the ENDF/B-IV cross-section library. Geometric corrections were calculated as a function of distance from the Be target for all of the nuclear reactions. This was done by integrating the neutron flux over the area of the foil:

$$\overline{\sigma\phi} = \frac{2\int_0^{\pi}\int_0^{x}\left[\frac{\sigma\phi(\psi)}{d^2}\right] r\, dr\, d\theta}{\int_0^{\pi}\int_0^{x} r\, dr\, d\theta} \qquad (4)$$

In Eq. 4, the denominator is the area of the foil (πx^2), ψ is the solid angle from the beam axis ($\tan\psi = r/R$), and $d^2 = r^2 + R^2$, R being the distance between the foil center and the Be target. The term $\sigma\phi(\psi)$ was determined by fitting the time-of-flight neutron spectral values times the activation cross sections (ENDF/B-IV) to a polynomial function of r/R. In the case of an isotropic neutron distribution, Eq. 4 reduces to:

$$\overline{\sigma\phi} = \sigma\phi(0)\left[\frac{1}{x^2}\ln\left(1 + \frac{x^2}{R^2}\right)\right] \qquad (5)$$

where the term in the brackets is referred to as a finite size correction and approaches $1/R^2$ when $x << R$. If $\sigma\phi(r/R) = \sum_{i=0}^{4} A_i(x/R)^i$, then it can be shown that:

$$\overline{\sigma\phi} = \frac{\sigma\phi(0)}{x^2}\left\{\left(A_0 - A_2 - A_4\right)\ln\left(1 + \frac{x^2}{R^2}\right)\right.$$

$$+ 2\left(A_1 - A_3\right)\left[\frac{x}{R} - \tan^{-1}\left(\frac{x}{R}\right)\right]$$

$$\left. + \left(A_2 - A_4\right)\left(\frac{x}{R}\right)^2 + \frac{2A_3}{3}\left(\frac{x}{R}\right)^3 + \frac{A_4}{2}\left(\frac{x}{R}\right)^4\right\} \qquad (6)$$

A computer program was used to evaluate this expression as a function of distance, R, for each of the reactions used in our experiment.

The geometric corrections for the irradiation in which E_d = 14 MeV are listed in Table I-12. These corrections were checked in two ways. First, the fission chamber was placed at various distances behind the Be target. The curve of yield *vs.* distance clearly deviated from $1/R^2$ and was also not as steep as the finite size correction in Eq. 5. The data are fit very well by the exact calculation of Eq. 6. The corrections were also checked by examining the activity ratios of Au and Al foils placed at various locations during the irradiation of our foil packets. Several important conclusions can be drawn from these data:

(1) The $1/R^2$ correction can be in error by as much as 4%.

(2) The error is largest at close geometry or when the correction must be made over a large distance, R.

(3) Different reactions have markedly different corrections, even within the same foil. For example, the (n,γ), (n,p), and (n,α) reactions all have negative errors (from $1/R^2$), whereas the (n,2n) errors are positive.

These corrections must not be underestimated in their importance to dosimetry data taken during the irradiation of materials since these irradiations are, by necessity, performed in very close geometry (*i.e.*, less than 1 cm between the Be and the foil materials). The corrections will thus be much greater than those shown in Table I-12. This was verified by placing a foil packet closer to the Be target: 2.01 cm rather than the 4.88 cm chosen for the calculations in Table I-12. The maximum deviations from $1/R^2$ were calculated to be as large as ±9% for the 2.01-cm case. Hence, care must be taken in actual irradiations to accurately define the geometry in order to apply the appropriate corrections. Accurate time-of-flight neutron spectral data are essential if corrections are to be made for finite size geometries.

Table I-12. Geometric Corrections for Foil Irradiations at E_d = 14 MeV for a Foil Diameter of 0.95 cm

Reaction	Distance from Be, mm[a]	$\frac{\overline{\sigma\phi}(R_o)}{\overline{\sigma\phi}(R)}$[b]	$\left(\frac{R}{R_o}\right)^2$[c]	% Dev.[d]
$^{197}Au(n,\gamma)$	48.69	1.000	1.000	-
$^{197}Au(n,2n)$	48.69	1.000	1.000	-
$^{27}Al(n,\alpha)$	48.78	1.000	1.000	-
$^{58}Ni(n,p)$	49.61	1.033	1.035	-0.2
$^{58}Ni(n,2n)$		1.043		+0.8
$^{235}U(n,f)$	50.47	1.070	1.071	-0.2
$^{47}Ti(n,p)$	51.10	1.095	1.098	-0.3
$^{46}Ti(n,p)$		1.094		-0.3
$^{48}Ti(n,p)$		1.099		+0.1
$^{238}U(n,f)$	51.84	1.126	1.130	-0.3
$^{238}U(n,\gamma)$		1.129		-0.1
$^{45}Sc(n,\gamma)$	52.32	1.148	1.151	-0.3
$^{45}Sc(n,2n)$		1.184		+2.8
$^{197}Au(n,\gamma)$	52.60	1.161	1.163	-0.2
$^{197}Au(n,2n)$		1.167		+0.3
$^{27}Al(n,\alpha)$	52.68	1.164	1.167	-0.2
$^{58}Fe(n,\gamma)$	52.81	1.173	1.173	0.0
$^{54}Fe(n,p)$		1.166		-0.6
$^{56}Fe(n,p)$		1.169		-0.3
$^{90}Zr(n,2n)$	53.26	1.235	1.193	+3.5
$^{63}Cu(n,\gamma)$	53.95	1.220	1.224	-0.4
$^{63}Cu(n,\alpha)$		1.218		-0.5
$^{65}Cu(n,2n)$		1.248		+2.0
$^{59}Co(n,\gamma)$	54.66	1.251	1.256	-0.4
$^{59}Co(n,p)$		1.248		-0.7
$^{59}Co(n,\alpha)$		1.253		-0.3
$^{59}Co(n,2n)$		1.296		+3.2
$^{115}In(n,n')$	55.09	1.269	1.277	-0.6
$^{93}Nb(n,2n)$	55.42	1.304	1.291	+1.0
$^{197}Au(n,\gamma)$	55.70	1.300	1.304	-0.4
$^{197}Au(n,2n)$		1.311		+0.5
$^{27}Al(n,\alpha)$	55.78	1.303	1.309	-0.5

[a] Distance computed to the centroid of the deuteron range in Be. The uncertainty here is about ±0.51 mm.

[b] $\overline{\sigma\phi}(R)$ calculated from Eq. 6. R_o was chosen as 48.8 mm or the distance to the front of the foil packet. The ratio is thus the correction factor such that all foils are at R_o.

[c] $(1/R_o)^2/(1/R)^2$ is the correction factor, neglecting finite size and the variations in the neutron flux and spectra.

[d] Percent deviation of the exact correction factor from $1/R^2$.

II. INTERLABORATORY LMFBR REACTION RATE (ILRR) PROGRAM
(R. J. Popek and R. R. Heinrich)

During the past year, Argonne National Laboratory's responsibilities in the ILRR program have been limited to the final compilation of fission-product production rates for ^{235}U, ^{238}U, ^{237}Np, and ^{239}Pu. Other participating laboratories have done similar fission-rate measurements; these laboratories include Hanford Engineering Development Laboratory (HEDL), National Bureau of Standards (NBS), and Aerojet Nuclear Corporation (ANC). Each participating laboratory also reports progress in the ILRR program by contributions to a report entitled, "Interlaboratory LMFBR Reaction Rate and Dosimetry Progress Report," which is compiled and distributed by HEDL.

The data presented in Tables II-1 and II-2 are the cumulative fractional fission yields for ^{95}Zr, ^{103}Ru, and ^{140}Ba for all of the four reporting laboratories from irradiations performed over a period from 1972 to 1974 at the CFRMF (Coupled Fast Reactivity Measurements Facility) located at Aerojet Nuclear Corporation (ANC), Idaho, the BIG-10 (a 10% enriched ^{235}U critical assembly) located at Los Alamos Scientific Laboratory (LASL), Los Alamos, New Mexico, and the NBS thermal cavity in Washington, D. C. All the foil irradiations were done with the NBS fission chamber and have been described previously.[17,18] In Table II-1, the data obtained from both CFRMF irradiations are averaged and are compared to the BIG-10 data. The average of both the CFRMF and BIG-10 data represents the ILRR fission yields and these are compared to the ENDF/B[19] recommended fast fission yields. As indicated, the consistency of the ILRR yields for both CFRMF and BIG-10 is excellent with the exception of ^{237}Np. The ^{237}Np yields are much more discrepant (6%) than the yields from the other isotopes. The average standard deviation for the yields of ^{235}U, ^{238}U, and ^{239}Pu obtained from BIG-10 was about 1.2%, whereas the standard deviation of the yields from CFRMF was less than 1%.

The agreement between the CFRMF and BIG-10 yields is within the experimental error in every case except one. The ^{103}Ru fission yield from ^{235}U is about 2.7% larger for BIG-10 than the yield for CFRMF. For the other fissionable isotopes, the ^{103}Ru yields are quite consistent for both CFRMF and BIG-10. Admittedly, it is somewhat surprising that such a difference might exist, but the excellent internal consistency of the data from the three participating laboratories for each facility does indicate that the relative uncertainty of the ^{103}Ru yield for ^{235}U exceeds that exhibited by the other fission products by about 2.5 times.

In Table II-2, the ILRR thermal yield results from the NBS thermal column irradiation are compared with those being compiled by Meek and Rider[19] for the ENDF/B compilation. Here, the Meek and Rider values for ^{95}Zr, ^{137}Cs, and ^{140}Ba fall within the uncertainties of the ILRR average, but the ^{103}Ru again appears to be somewhat discrepant.

Presented in Table II-3 is a comparison of the ratios of ^{235}U fast-neutron yields to thermal-neutron yields for the ILRR data and the Meek and Rider recommendation. Again the agreement between the ILRR data and the Meek and Rider values is excellent for ^{95}Zr and ^{140}Ba, but poor for ^{103}Ru. Thus, the large discrepancy for ^{103}Ru appears to indicate that the production of this fission product in ^{235}U is more sensitive to changes in neutron energy than are the others.

Table II-1. Summary of ILRR Cumulative Fractional Fission Yields for Fast Reactor Spectra

Fission Product	BIG-10 1974, %	CFRMF 1974, %	CFRMF 1972, %	CFRMF Avg., %	CFRMF Avg./ BIG-10	ILRR Avg. (BIG-10, CFRMF), %	ENDF/B Recom. Fast Yield, %	ILRR/ (ENDF/B)
				Neptunium-237 Yields				
^{95}Zr	5.97 ±2.6[a]	5.71 ±3.4	6.05 ±3.8	5.88 ±4.0	0.985	5.93 ±4.0		
^{103}Ru	5.94 ±5.0	5.91 ±4.6	5.75 ±4.2	5.83 ±5.0	0.981	5.89 ±5.0		
^{140}Ba	5.68 ±3.3	5.75 ±2.5	5.79 ±2.1	5.77 ±2.5	1.016	5.73 ±3.0		
				Uranium-235 Yields				
^{95}Zr	6.45 ±2.1	6.44 ±2.2	6.43 ±2.1	6.44 ±2.1	0.998	6.45 ±2.1	6.38 ±2.0	1.011
^{103}Ru	3.38 ±3.9	3.30 ±3.9	3.25 ±4.2	3.29 ±3.9	0.973	3.35 ±5.0	3.24 ±2.0	1.034
^{140}Ba	6.07 ±1.8	6.07 ±1.9	6.04 ±1.8	6.06 ±1.8	0.998	6.07 ±1.8	6.12 ±1.4	0.992
				Uranium-238 Yields				
^{95}Zr	5.21 ±2.5	5.17 ±2.5	5.16 ±2.5	5.17 ±2.5	0.992	5.20 ±2.5	5.12 ±2.0	1.016
^{103}Ru	6.37 ±4.0	6.31 ±4.1	6.28 ±4.3	6.30 ±4.0	0.998	6.35 ±4.0	6.22 ±2.0	1.021
^{140}Ba	6.01 ±2.1	5.97 ±2.3	5.96 ±3.8	5.97 ±2.3	0.993	6.00 ±2.1	5.95 ±2.0	1.008
				Plutonium-239 Yields				
^{95}Zr	4.79 ±2.2	4.80 ±2.3		4.80 ±2.3	1.002	4.79 ±2.2	4.68 ±2.8	1.024
^{103}Ru	7.11 ±3.9	7.07 ±4.0		7.07 ±3.9	0.994	7.10 ±3.9	6.69 ±2.0	1.061
^{140}Ba	5.31 ±1.9	5.34 ±2.1		5.34 ±2.1	1.006	5.32 ±1.9	5.35 ±2.0	0.994

[a]Standard deviations are expressed as percent of yield.

Table II-2. Comparison of Measured Yields for the NBS Thermal Column Irradiation With ENDF/B Thermal Yields

Fission Product	ILRR Weighted Mean Yield, %	ENDF/B (Meek & Rider, Recom. Thermal, June 1976),[19] %	ILRR/ (ENDF/B)
^{95}Zr	6.50 ± 2.5[a]	6.443 ± 1.4	1.009 ± 0.029
^{103}Ru	3.02 ± 4.1	3.146 ± 2.0	0.960 ± 0.046
^{137}Cs	6.12 ± 2.4	6.236 ± 0.7	0.981 ± 0.025
^{140}Ba	6.22 ± 2.3	6.291 ± 1.4	0.989 ± 0.027

[a]Standard deviations are expressed as percent of yield.

Table II-3. Uranium-235 Fast/Thermal Yield Ratios

^{235}U Fission Product	ILRR Fast/Thermal Ratio	ENDF/B Fast/Thermal Ratio	Discrepancy ILRR *vs.* ENDF/B, %
^{95}Zr	0.992	0.990	0.2
^{103}Ru	1.109	1.029	7.8
^{140}Ba	0.976	0.972	0.4

III. DEVELOPMENT OF LIQUID SCINTILLATION NEUTRON DETECTORS

(L. R. Greenwood, N. R. Chellew, and R. R. Heinrich)

Work at Argonne National Laboratory has been responsible for the development of improved neutron detection techniques that are applicable to a number of research areas. Currently, the experience and expertise gained at ANL in neutron detection techniques is being applied to the development of a means for detecting a neutron source whose intensity at the point of detection is comparable to the intensity of the ambient neutron background levels. Such low-intensity measurements will be complicated by the presence of background neutrons that result predominantly from cosmic-ray interactions with surrounding materials. The major source of background neutrons occurs at the air-land interface, where the density of atoms that can interact with cosmic rays is the greatest. Additionally, any massive amount of material surrounding the detector represents a source of cosmic-ray interaction which could potentially raise the neutron and the gamma-ray background. Direct cosmic-ray interactions within the detector can also occur, but the probability of such interactions is considered to be small owing to the high energy of the cosmic radiation and the low proton flux levels.

Thus, the ideal detector for this application should possess the following characteristics: (1) high neutron-detection efficiency, (2) large areas with uniform sensitivity, (3) small total volume, (4) some means for discriminating between source neutrons and background neutrons and gamma rays, and (5) low-mass, low-Z material surrounding the detector. Of all currently available neutron-detection techniques, ^{10}B-loaded liquid scintillation (BLLS) detectors appear to be the most attractive.

The solution selected contains ^{10}B-enriched trimethyl borate (TMB), 1-methylnaphthalene (MN), and 9, 10-diphenylanthracene (DPA). The exact composition of the MN-TMB-DPA mixture will depend on the performance observed for a selected cell size.

A. Preparation of Scintillator Solutions

A critical problem encountered in the development of the ^{10}B-loaded detectors has been the purity of ingredients used in the scintillation mixture. In order to achieve satisfactory detector performance, we have had to develop the capability of purifying the components in our laboratory. This was prompted by the unsatisfactory past performance of commercial vendors and by the fact that, initially, only small amounts of these materials were to be used.

The only commercially available MN was of very poor quality, characterized by a deep yellow color with very strong absorption bands in the region of 400 nm. Successful purification of this MN was achieved by a three-step procedure which consisted of two activated-charcoal treatments, followed by a vacuum distillation. This procedure resulted in very pure MN. Earlier efforts in which activated charcoal was used alone were moderately successful in that impurities centered about the 410-nm band were removed, but broad-band impurities still remained. The results of absorption tests of treated and untreated MN, using 1-cm spectrophotometric cells, are illustrated in Fig. III-1; the charcoal-treated and vacuum-distilled material shows no detectable impurity (Curve D).

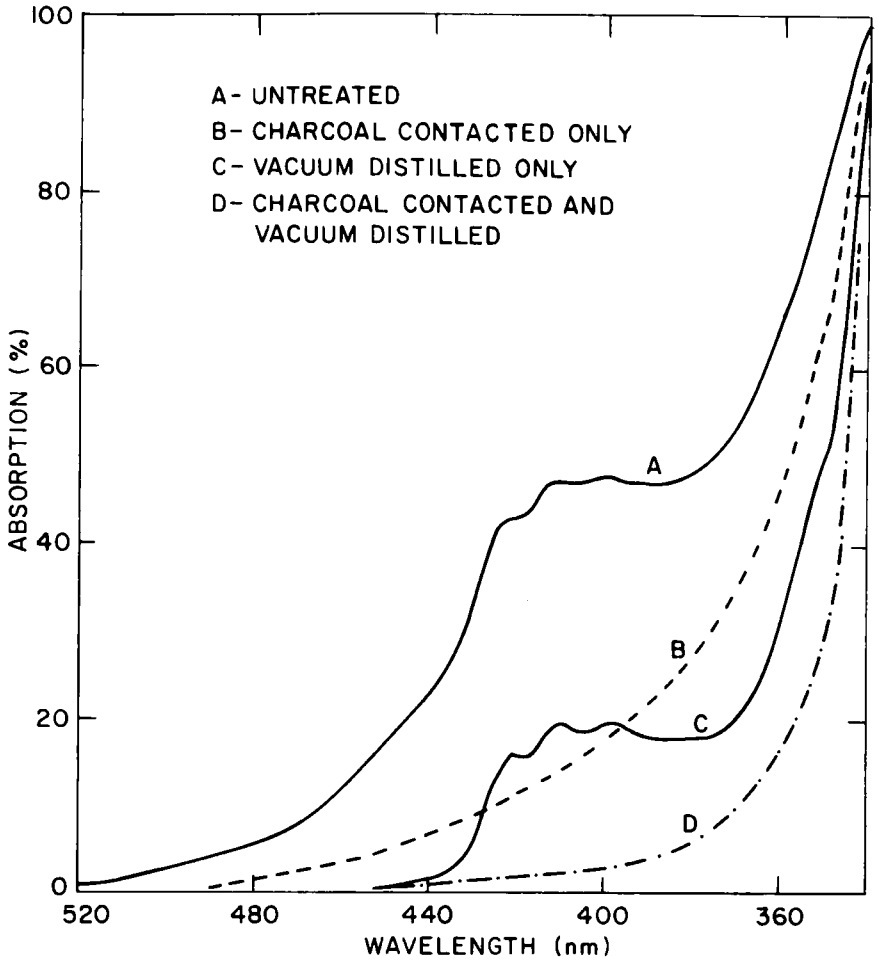

Fig. III-1. Transparency Measurements for Undiluted 1-Methylnaphthalene in 1-cm Cells as a Function of Purification Treatment

The purified MN was used to make several boron-loaded cells by combining it with trimethylborate (TMB) and 9, 10-diphenylanthracene (DPA). The purity of the commercial TMB was acceptable, but the DPA needed to be purified in our laboratory.[17] The performance of these cells is presented in Table III-1.

The solution labeled MNBI was made by using MN that had not been vacuum distilled. The solution MNBII was of similar composition except that purified MN was used. The relative light output of MNBII increased by 68% over that of MNBI, and the pulse-shaped discrimination (PSD) figure-of-merit, M (M is defined as the time separation between the neutron and gamma-ray peaks divided by the sum of the full widths at half-maximum), increased to 0.7, as compared with an M value of less than 0.4 for MNBI.

In Table III-1, the MN results are also compared with those of a cell containing toluene and naphthalene. The solution labeled MBIV consisted of toluene (30.6%), TMB (46.5%), naphthalene (21.7%), and DPA (1.2%); MBIV exhibited the best performance, as compared with the Jackson-Thomas[20] mixture (similar to that provided by Nuclear Enterprises, Inc., and labeled NE321).

Table III-1. Test Results for MN-Based, Boron-Loaded Scintillators (cells were 1-cm thick)

Mixture	Concentration, wt %			Relative Light Output[d]	PSD M[e]
	1-MN[a]	TMB[b]	DPA[c]		
MNBI	19.9[f]	79.6	0.50	0.25[f]	<0.4
MNBII	21.2	78.3	0.53	0.42	0.7
MNBIII	27.4	71.7	0.92	0.48	0.8
MNBIV	50.7	48.7	0.62	0.63	1.0
MBIV	(toluene + TMB + naphthalene + DPA)			0.60	1.0

[a] 1-Methylnaphthalene.

[b] Trimethylborate.

[c] 9, 10-diphenylanthracene (not scintillation grade).

[d] Relative to light output from archival NE321.

[e] M represents the figure-of-merit for the pulse-shape discrimination (PSD) and is defined as the time separation between neutron and gamma-ray peaks divided by the sum of the full widths at half-maximum.

[f] The MN was not vacuum-distilled in this case, but was charcoal-treated.

The solution labeled MNBII exhibited only 70% of the light output of MBIV; however, the boron loading was 68% higher for MNBII, as compared with MBIV loading. Increasing the DPA concentration of MNBII was found to increase the light output to 80% of that of MBIV, as shown by a comparison of MNBIII with MNBII. Solution MNBIV represents a solution in which the boron concentration was made equivalent to that of the toluene solution (MBIV), and as indicated, slightly better results were obtained.

High-purity commercial DPA has been obtained from Koch Light Laboratories (United Kingdom). Spectral absorbance tests and liquid scintillator cell performance tests have shown this material to be of excellent quality. Results of cell performance tests in which this DPA was used are shown in Table III-2. The solution labeled MBV is very close in composition to the Jackson-Thomas formula and the archival commercial solution, NE321. The performance of the MBV solution is identical to that of NE321, whereas previously, using impure materials, we were able to achieve only about 60% of the light output of NE321 and a M $\approx$1.0 for a similar mixture of ingredients. The solution labeled MNBV contains 1-methylnaphthalene (MN) instead of toluene and naphthalene. The light output for this solution is about 15% higher than that for NE321, which has a slightly lower boron loading. These results are added evidence of improved performance when MN is used.

Table III-2. Test Results for Boron-Loaded Scintillators in 1-cm-Thick Cells

Mixture	Composition, wt %					Relative Light Output	PSD M[d]
	TMB[a]	Toluene	1-MN[b]	Naphthalene	DPA[c]		
MBV	46.1	34.7	-	18.1	1.17	1.00	1.2
MNBV	48.6	-	50.2	-	1.14	1.15	1.2
NE321[e]	46.5	30.6[f]	-	21.7	1.2	1.00	1.2

[a]Trimethyl borate.

[b]1-Methylnaphthalene (purified in house).

[c]9, 10-diphenylanthracene (Koch-Light).

[d]M represents the PSD figure-of-merit; for definition of M, see Table III-1.

[e]Exact concentrations not known.

[f]Xylene used instead of toluene.

A new supply of trimethylborate (TMB) was obtained from Eagle-Picher Industries (EPI), Inc., and the results of performance tests of cells containing this material are compared with those of cells containing on-hand material in Table III-3. We have also tested the EPI sample of TMB in combination with MN, instead of toluene and napthalene, and these results are also presented in Table III-3. Again, the use of MN allows a substantially higher boron loading, as can be seen by comparing solutions MNBVI, MNBVII, and MNBVIII in which the TMB concentration increases from 30.2% to 79.7%. The final MN solution tested, MNBVIII, with a nearly 80% TMB content, had nearly the same light output as the toluene-naphthalene mixtures (MBIX and MBX), which contained only 46% TMB. All of the solutions tested in Table III-3 exhibited good pulse shape discrimination (PSD) with figures-of-merit (M) values between 1.0 and 1.2. As a result of these tests, it appears that a solution similar in composition to MNBVII would be the best choice for a prototype detector because of its high boron loading and performance. However, the exact composition used in a prototype system will depend on the performance in large volume cells. Preliminary tests of the Jackson-Thomas formula in a 5.1-cm-dia by 5.1-cm-long cell coupled to a single 5.1-cm dia phototube (RCA-8850) indicate less than a 30% drop in light output as compared to the 1 cm-thick cell.

A mixture, MNBX, which contained MN and toluene, was also tested; the test results are shown in Table III-3. The dilution with toluene did not affect the light output and may have helped to increase the cell stability at low temperatures. Solutions with various concentrations of MN will now be tested to decide on the best solution.

Table III-3. Test Results for Boron-Loaded Liquid Scintillators in 1-cm-Thick Cells

Mixture	Concentration, wt %					Relative Light Output
	TMB[a]	Toluene	1-MN[b]	Naphthalene	DPA[c]	
NE321[d]	46.5[e]	(30.6)[f]	-	21.7	1.20	1.00
MBIX	45.5[g]	35.2	-	18.2	1.10	1.00
MBX	46.3[h]	34.5	-	18.0	1.12	1.00
MNBVI	30.2[h]	-	68.6	-	1.17	1.24
MNBIX	49.1[g]	-	49.9	-	1.0	1.10
MNBX	49.0[g]	19.7	30.2	-	1.0	1.04
MNBVII	59.5[h]	-	39.4	-	1.16	1.00
MNBVIII	79.7[h]	-	19.5	-	0.83[i]	0.96

[a] Trimethyl borate.

[b] 1-Methylnaphthalene (purified in house).

[c] 9, 10-diphenylanthracene (Koch-Light).

[d] Exact concentrations unknown.

[e] TMB supplied by Nuclear Enterprises, Inc., San Carlos, California.

[f] Xylene used instead of toluene.

[g] TMB supplied by Rho Chemical Co., Inc., Joliet, Illinois.

[h] TMB supplied by Eagle-Picher Industries, Inc., Miami, Okalahoma.

[i] The solubility limit of DPA in 1-MN was reached in this case.

B. Performance Tests of Large Volume Detectors

Measurements of the light output and pulse shape discrimination (PSD) for a 5.1-cm-dia by 15.2-cm-long cylindrical cell filled with ^{10}B-loaded solution have been encouraging. The solution consists of 51.5% trimethylborate (92% ^{10}B), 47.5% 1-methylnaphthalene, and 1% diphenylanthracene. The cell is viewed at each end by two 5.1-cm-dia RCA 8850 photomultiplier tubes. A collimated beam of gamma rays was moved along the axis of the cell in order to measure the light intensity versus gamma-ray position. The results are shown in Fig. III-2 and indicate that the mean free path for light through the mixture is about 12.7 cm; that is, the light received by a single phototube is

$$I(d) = I_o e^{-\lambda d}$$

where I(d) is the intensity received when the gammas are incident at d centimeters from the face of the phototube and $\lambda = 1/12.7$ cm. When both tubes are used, the light intensity is the sum of the individual intensities

$$I(d) = e^{-\lambda L/2} \cosh(\lambda x)$$

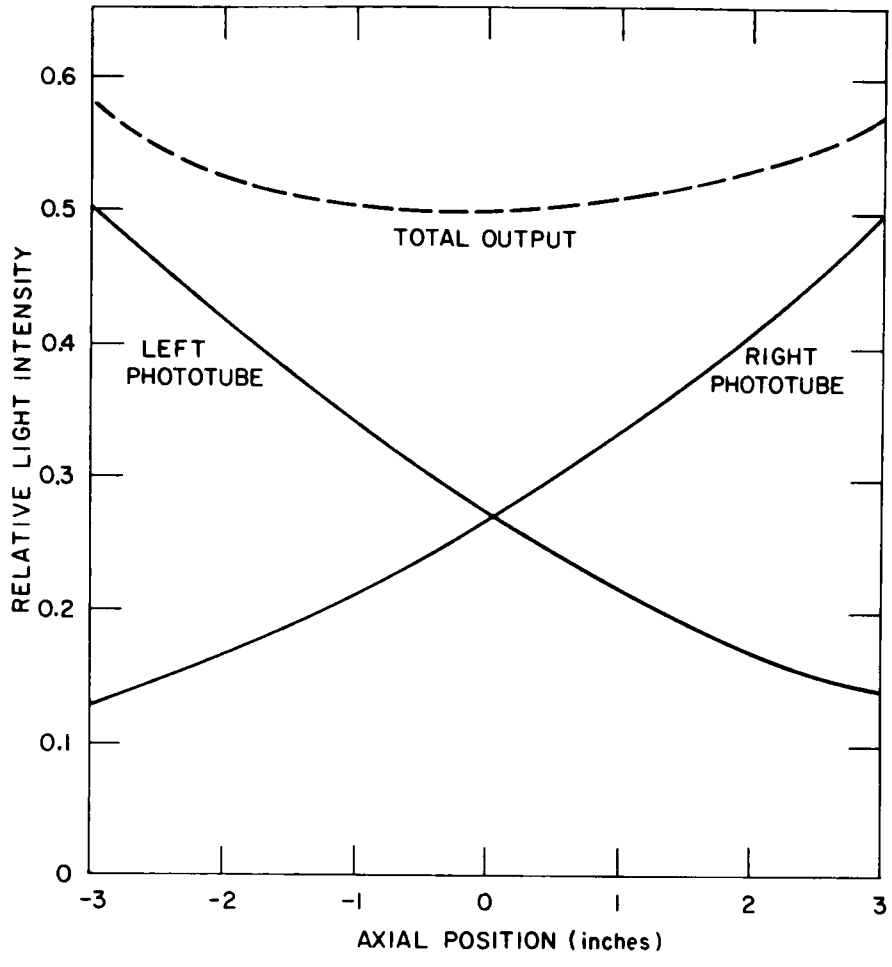

Fig. III-2. Light Intensity *vs.* Axial Position for 5.1-cm-dia by 15.2-cm-long Cell Filled with ^{10}B-Loaded Solution Coupled to Two RCA-8850 Phototubes.

normalized so that the total intensity is equal to 1 for a very short cell, where L is the total length (cm) of the cell and x is the distance (cm) away from the cell center (x = 0). The intensity seen at the center of the cell is given by $I(0) = e^{-\lambda L/2}$ and the average intensity, integrated over the length of the cell, is given by

$$\langle I \rangle = \frac{2e^{-\lambda L/2} \sinh (\lambda L/2)}{L\lambda}$$

The results obtained with the equations given above are illustrated in Table III-4 for various cell lengths (L).

It should be pointed out that these values were obtained by measuring the peak of the Compton electron energy distribution and not the half-height of the distribution. This procedure, of course, results in more attenuation or a shorter mean free path than would have been the case if a half-height distribution had been used. Moreover, the equations are inexact at very short

Table III-4. Relative Light Intensity *vs.* Cell Length

L, cm	I(0) (Center)	I(L/2) (Ends)	<I> (Average)
2.54	0.90	0.91	0.91
5.08	0.82	0.84	0.83
10.16	0.67	0.73	0.69
15.24	0.55	0.65	0.58
20.32	0.45	0.60	0.50

distances owing to the more rapid attenuation of the short wavelength portion of the emission spectrum.

These results were checked by measuring 5.08-cm-long and 15.24-cm-long cells. The measured ratio of the total intensities agreed very well with our calculations, as shown in Table III-5.

Table III-5. Relative Light Intensities for a 2-Inch-Thick Cell

L (cm)	I(0) (Expt.)	I(0) (Calculated)	M, PSD-Figure-of-Merit
5.08	0.85	0.82	1.05
10.16	-	0.67	-
15.24	0.55	0.55	0.90

The deterioration in PSD performance caused by the increased volume of cell solution is not judged to be severe; however, field testing will be required to fully assess the importance of this effect. It should also be pointed out that the PSD performance can always be improved by raising the lower level discriminator, thereby making a 15.2-cm cell respond like a 10.2-cm or 5.1-cm cell at the sacrifice of some efficiency.

C. Low-Temperature Tests of Scintillation Mixtures

Reduction of the temperature of liquid scintillation mixtures that are being considered for a neutron detector could change the solute concentrations (9, 10-diphenylanthracene and naphthalene in ^{10}B-loaded solutions) to a point that might affect energy transfer efficiency. Tests were carried out in which three types of ^{10}B-enriched trimethylborate mixtures encapsulated in 1-cm spectrophotometer cells were cooled in a refrigerator at various temperatures below the temperature of solution preparation ($\sim$25°C). A thermometer, placed immediately adjacent to the cell, was used for temperature measurement, and the cells were removed after at least 4 hours of cooling to determine whether solute precipitation had occurred. Results of these tests are summarized in Table III-6.

Table III-6. Effect of Cooling on B-Loaded Scintillation Mixtures

Mixture	Concentration, wt %					Comments
	TMB[a]	TOL[b]	MN[c]	NPT[d]	DPA[e]	
MBX	46.3	34.6	-	18.0	1.1	Solute precipitation evident at 4 ± 3°C (∿40°F).
MNBIX	49.1	-	49.9	-	1.0	No solute precipitation evident at -17 ± 3°C (∿1°F).
MNBX	49.0	19.7	30.2	-	1.1	No solute precipitation evident at -17 ± 3°C (∿1°F).

[a] ^{10}B-enriched trimethylborate (mp, -29°C).

[b] Toluene (mp, -95°C).

[c] 1-Methylnapthalene (mp, -30.8°C).

[d] Naphthalene (mp, 80.2°C).

[e] 9, 10-diphenylanthracene (mp, 247°C).

From these tests, it is evident that for scintillation solutions containing approximately equal boron-10 loadings, those containing naphthalene are less stable at subambient temperatures than those prepared with 1-methylnapthalene. In the MBX solution, which contained dissolved naphthalene, precipitation was observed at about 4°C. As the temperature was decreased from 4 to 0°C, the volume of precipitated white crystals grew considerably. However, precipitation of very light yellow 9, 10-diphenylanthracene crystals was not visible in any of the tests.

D. ^{6}Li-Loaded Scintillator Systems

Although ^{10}B-loaded solutions have shown the most potential for use in a demonstration neutron detector, a limited effort was continued during the past year to investigate ^{6}Li-loaded solutions. The major advantages of ^{6}Li-loaded solutions are (1) better light output, (2) superior pulse-shape discrimination (PSD) performance, and (3) lesser sensitivity to ambient gamma background during operation. A major disadvantage is the low solubility of scintillator-compatible lithium compounds in conventional scintillation solvents; thus, to achieve the efficiency of the ^{10}B-loaded cells (which contain ∿5 wt % ^{10}B), the volume of solution used in the ^{6}Li system would have to be substantially increased. Previous work with ^{6}Li-salicylate (LISA)-loaded solutions provided evidence that severe light quenching occurred when water was added to dioxane to increase LISA loading.

The importance of 9, 10-diphenylanthracene (DPA) and 1-methylnapthalene (MN) or naphthalene (NPT) in achieving better performance with methyl borate solutions has already been demonstrated. We therefore restricted our initial

investigation to scintillation mixtures containing LISA, DPA, and MN or NPT, and scintillation solvents for these materials. In each case, methanol was used as one component of the solvent because LISA is highly soluble in methanol and because methanol is not an excessive light quencher in scintillation solutions. The approximate solubilities of LISA, DPA, and NPT in liquids used for preparation of the test solutions are given in Table III-7. From this table, it is apparent that all LISA-methanol systems require additional solvent(s) if the DPA concentration in the final solution is to be maintained between 0.7 and 1.2 wt % (a desirable concentration for systems utilizing DPA as a wavelength shifter).

Table III-7. Solubility of LISA, DPA, and NPT in Selected Scintillation-Compatible Liquids

Solute	Solvent	Approximate Solubility, wt %
LISA	Toluene	negligible at 25°C
LISA	1-Methylnaphthalene	<0.1 at 25°C
LISA	Methanol	68 at 25°C
DPA	Toluene	1.35 at 25°C
DPA	1-Methylnaphthalene	1.75 at 25°C
DPA	Methanol	<0.03 at 25°C
NPT (Ref. 21)	Toluene	28.7 at 15°C
NPT	1-Methylnaphthalene	(very soluble)
NPT (Ref. 21)	Methanol	19.5 at 15°C

Stability test data on mixtures containing LISA are given in Table III-8. In most cases, the mixtures were prepared by first adding DPA in increments to other constituents of the solution until no additional DPA would dissolve. A final step involved adjusting the concentration of the solutes (LISA and DPA) by the addition of liquids (methanol, toluene, MN) until the solution appeared clear. Mixtures A, B, and C were prepared with methanol-toluene solvents. Although the initial performance of C was very good, the mixture was not stable. Mixtures D and E were prepared with MN substituted for toluene and NPT. Although as much as 20.7 wt % LISA could be dissolved in this system, the solutions became cloudy shortly after preparation and would accept only ~0.2 wt % DPA. Mixture F was prepared to determine whether the addition of toluene to a methanol-MN-LISA mixture would increase the solubility of DPA. As indicated in Table III-8, this solution was stable at room temperature but would accept only 0.13 wt % DPA.

The preliminary tests of various nonaqueous LISA mixtures suggest that, for dissolving sufficient DPA for good performance (a minimum of ~0.7 wt %), mixtures containing toluene-methanol and NPT may be superior to mixtures containing MN. Future plans call for evaluating the effect of NPT concentration

Table III-8. Stability Tests of Nonaqueous ^{6}Li-Loaded Scintillator Mixtures

Test	LISA	Methanol	Toluene	MN	NPT	DPA	Mixture Stability at 25°C
A	4.23	32.54	57.75	-	4.83	0.65	Stable
B	7.10	29.00	47.02	-	16.02	0.86	Unstable after several hours
C	7.52	23.73	54.95	-	13.09	0.71	Unstable after several hours
D	11.30	59.15	-	29.35	-	0.20	Unstable after several hours
E	20.68	54.65	-	24.50	-	0.17	Unstable after several hours
F	16.19	42.75	21.75	19.18	-	0.13	Stable

on the performance of toluene-methanol solutions containing ∿7 wt % LISA and 0.7 wt % DPA. If a mixture can be made that is stable at room temperature, a 5.1-cm-dia by 15.2-cm-long cell will be used in tests to compare the performance of the ^{6}Li-loaded solution with our present ^{10}B-loaded solution.

REFERENCES

1. D. M. Parkin, N. D. Dudey, R. R. Heinrich, and M. J. Fluss, *A Preliminary Neutron Foil Dosimetry Characterization of the BLIP Neutron Facility*, Brookhaven National Laboratory, USAEC Report BNL-50412 (1973).

2. M. Kaminsky, J. Peavey, and S. K. Das, Bull. Amer. Phys. Soc. *19*, 31 (1974).

3. M. Kaminsky, J. Peavey, and S. K. Das, Phys. Rev. Letters *32*, 599 (1974).

4. O. K. Harling, M. T. Thomas, R. L. Bradzinski, and L. A. Rancitelli, Phys. Rev. Letters *34*, 1340 (1975).

5. C. Wong, J. D. Anderson, P. Brown, L. F. Hansen, J. L. Kammerdiener, C. Logan, and B. Pohl, *Livermore Pulsed Sphere Program: Program Summary through July 1971*, Lawrence Livermore Laboratory, USAEC Report UCRL-51144 (1971).

6. J. L. Fowler and J. E. Brolley, Jr., Rev. Mod. Phys. *28*, 103 (1956).

7. B. A. Magurno, ed., *ENDF/B-IV Dosimetry File*, Brookhaven National Laboratory, National Neutron Cross Section Center Report BNL-NCS-50446 (ENDF-216) (1975).

8. D. R. Nethaway, *Cross Sections for Several (n,2n) Reactions at 14 MeV*, Nucl. Phys. *A190*, 635 (1972); and private communication.

9. S. F. Mughabghab, A. Prince, M. D. Goldberg, R. R. Bhat, and S. Pearlstein, *Evaluation of Neutron Cross Sections of* ^{197}Au, Brookhaven National Laboratory Report BNL 50439 (ENDF-215) (1974).

10. Z. T. Bödy and J. Csikai, *Recommended Values of (n,2n) Cross-Sections at 14.7 MeV*, Atom. Energy Rev. *11*, 153 (1973).

11. G. R. Odette and D. R. Doiron, Nucl. Technol., *29*, No. 3, 346 (1976).

12. J. Lindhard, M. Scharff, and H. E. Schiott, Mat. Fys. Medd, Dan, Vid. Selsk. *33*, No. 14 (1963).

13. G. Kinchin and R. Pease, Prog. in Physics *18*, 1 (1955).

14. A. N. Goland, D. H. Gurinsky, J. Hendrie, J. Kukkonen, T. Sheehan, and C. L. Snead, Jr., *Production and Use of Li(d,n) Neutrons for Simulation of Radiation Effects in Fusion Reactors*, Proc. Int. Conf. on Radiation Test Facilities for the CTR Surface and Materials Program, Argonne National Laboratory, Argonne, Ill., p. 371 (July 1975).

15. D. M. Parkin, Los Alamos Scientific Laboratory, private communication.

16. P. Grand, K. Batchelor, J. P. Blewett, A. Goland, D. Gurinsky, J. Kukkonen, and C. L. Snead, Jr., Nucl. Technol. *29*, No. 3, 327 (1976).

17. R. R. Heinrich, N. D. Dudey, L. R. Greenwood, N. R. Chellew, R. J. Popek, R. L. Malewicki, F. A. Cafasso, and L. Burris, *Chemical Engineering Division Fast Neutron Dosimetry Annual Report*, Argonne National Laboratory Report ANL-75-49, July 1974-June 1975, p. 17.

18. J. A. Grundl, D. M. Gilliam, N. D. Dudey, and R. J. Popek, Nucl. Technol. *25*, No. 2, 237 (1975).

19. M. E. Meek and B. F. Rider, General Electric Co., private communication.

20. H. E. Jackson and G. E. Thomas, Rev. Sci. Instrum. *36*, 419 (1965).

21. Donaldson, N., *The Chemistry and Technology of Naphthalene Compounds*, Edward Arnold Ltd., London (1958).

Distribution for ANL-76-104

Internal:

J. A. Kyger
C. E. Till
R. E. Rowland
D. W. Cissel
R. J. Teunis
P. R. Fields
G. T. Garvey
C. C. Baker
M. Ader
J. E. Battles
G. J. Bernstein
P. E. Blackburn
M. Blander
H. L. Brown
L. Burris (4)
F. A. Cafasso
M. G. Chasanov
N. R. Chellew
L. L. Cuba
P. T. Cunningham
A. M. Essling
J. P. Faris
A. K. Fischer
I. M. Fox
T. J. Gerding
H. T. Goodspeed
L. R. Greenwood
R. R. Heinrich (6)
M. I. Homa
B. R. Hubble
L. J. Jardine
C. E. Johnson
G. K. Johnson
S. A. Johnson
G. M. Kesser
E. T. Kucera
G. H. Kucera
B. J. Kullen
L. Leibowitz
R. N. K. Lo
R. L. Malewicki
A. F. Melton
R. J. Meyer
R. J. Popek
D. J. Rokop
J. Royal
W. A. Shinn
S. Siegel
S. B. Skladzien
G. E. Staahl
D. V. Steidl
M. J. Steindler
B. S. Tani
R. E. Telford
L. E. Trevorrow
S. Vogler
C. G. Wach
R. J. Armani
R. Larsen
R. Oldham
D. Meneghetti
E. R. Ebersole
A. B. Krisciunas
ANL Contract Copy
ANL Libraries (5)
TIS Files (6)

External:

ERDA-TIC, for distribution per UC-20c (215)
Manager, Chicago Operations Office
Chief, Chicago Patent Group
President, Argonne Universities Association
Chemical Engineering Division Review Committee:
R. C. Axtmann, Princeton U.
R. E. Balzhiser, Electric Power Research Inst.
J. T. Banchero, U. Notre Dame
D. L. Douglas, Gould Inc.
P. W. Gilles, U. Kansas
R. I. Newman, Allied Chemical Corp.
G. M. Rosenblatt, Pennsylvania State U.